October 2022

Manganese Bioavailability Drives Organic Matter Transformations Across Oxic-Anoxic Interfaces via Biotic and Abiotic Pathways

Nathan A. Chin
University of Massachusetts Amherst

MANGANESE BIOAVAILABILITY DRIVES ORGANIC MATTER TRANSFORMATIONS ACROSS OXIC-ANOXIC INTERFACES VIA BIOTIC AND ABIOTIC PATHWAYS

A Thesis Presented

by

NATHAN A. CHIN

Submitted to the Graduate School of the

University of Massachusetts Amherst in partial fulfillment

of the requirements for the degree of

MASTER OF SCIENCE

SEPTEMBER 2022

Plant and Soil Science

MANGANESE BIOAVAILABILITY DRIVES ORGANIC MATTER TRANSFORMATIONS ACROSS OXIC-ANOXIC INTERFACES VIA BIOTIC AND ABIOTIC PATHWAYS

A Thesis Presented

by

NATHAN A. CHIN

Approved as to style and content by:

_____

Marco Keiluweit, Chair

_____

Baoshan Xing, Member

_____

Matthew Winnick, Member

_____

Baoshan Xing, Department Head
Stockbridge School of Agriculture

ACKNOWLEDGEMENTS

I would like to thank and acknowledge my committee Marco Keiluweit, Matthew Winnick, and Baoshan Xing for their patience and feedback while working with me. I would also like to thank Morris E. Jones, Jacob Zeigler, and especially Marco Keiluweit for their involvement in this work. Your expertise, assistance, and guidance crafted the foundation for this project and allowed me to see it to completion. A special thanks to my family and friends for their understanding and encouragement throughout the years. I would also like to thank Sarah Weis, Morris E. Jones, and Hamid Mashayekhi for their assistance and expertise on operating the TOC and MP-AES. Additional to Jay Dynes, Tom Regier, Yongfeng Hu, and Mohsen Shakouri for their help on both operating and processing samples on the SXRMB and SGM beamlines at the Canadian Light Source and Jürgen Thieme for his help at the SRX beamline at the Brookhaven National Laboratory.

ABSTRACT

MANGANESE BIOAVAILABILITY DRIVES ORGANIC MATTER TRANSFORMATIONS ACROSS OXIC-ANOXIC INTERFACES VIA BIOTIC AND ABIOTIC PATHWAYS

SEPTEMBER 2022

NATHAN A. CHIN

B.S., CORNELL UNIVERSITY, ITHACA, NY

M.S., UNIVERSITY OF MASSACHUSETTS, AMHERST, MA

Directed by: Professor Marco Keiluweit

Soil organic matter decomposition is a critical process that affects nutrient cycling, CO_2 emissions, and carbon storage in terrestrial environments. Recent evidence suggests reactive manganese (Mn) phases, potent oxidants that depolymerize compounds like lignocellulose in soil organic matter, act as critical drivers of organic matter decomposition in soil and sediment environments. Furthermore, oxic-anoxic interfaces (OAIs) have been shown to be crucial hotspots for the formation of reactive Mn(III) species and associated organic matter degradation. However, the extent to which microbially mediated Mn(III) formation and subsequently Mn(III)-driven organic matter oxidation depends on Mn availability remains largely unknown. Additionally, the relative contributions between abiotic and biotic Mn-mediated organic matter oxidation pathways have been poorly quantified. In this study, we quantified the impact of Mn availability on Mn-mediated particulate organic carbon (POC) oxidation across the redox gradient and the specific contributions of abiotic and biotic reactions. To accomplish this, we

established soil redox gradients in diffusion reactors and varied Mn(IV) oxide concentrations in the anoxic zone. The ensuing reductive mobilization of Mn(IV) oxides in the anoxic zone was meant to manipulate Mn(II) supply towards the OAI. The addition or exclusion of microbial inoculum allowed us to examine the abiotic contributions to Mn translocation and POC oxidation. Mn(II) translocation, Mn(III) formation, and C transformations across the redox gradient were quantified over a 12-week incubation period. Wet-chemical extractions combined with Mn XANES indicated that reactive Mn(III) formation at OAIs increased with enhanced Mn availability. Comparison of inoculated and uninoculated treatments revealed microbial Mn oxide reduction to be the critical driver of Mn translocation to oxic-anoxic interfaces. Subsequent enhanced Mn availability at the OAI enhanced POC oxidation and increased CO_2 production rates due to enhanced microbial translocation and primarily attributed to microbially mediated Mn(III) formation. Our study emphasizes the importance of Mn(III)-mediated C oxidation across OAIs and its dependence on the provision of Mn(II) through microbial Mn reduction. Combined, our results show Mn–C coupled cycling across redox gradients as a critical biogeochemical process that has profound impacts on ecosystem scale soil C storage and CO_2 fluxes.

TABLE OF CONTENTS

LIST OF TABLES

LIST OF FIGURES

Supplementary Figures List:

S.I. Figure 7 Sequential extraction results for Fe.

CHAPTER 1

INTRODUCTION

Global importance of Mn in decomposition

Soil organic matter is the largest and most dynamic terrestrial soil carbon (C) pool (Scharlemann et al. 2014). Accordingly, the decomposition of soil organic matter is a crucial mechanism that controls nutrient release and cycling within terrestrial ecosystems, which in turn are critical for plant growth (Hättenschwiler et al. 2005). Soil organic matter decomposition also impacts terrestrial C fluxes, thereby influencing the release of CO_2 (Heimann and Reichstein 2008) and potentially creating positive feedback loops that exacerbate climate change (Davidson and Janssens 2006). Understanding the factors affecting soil organic matter decomposition are, therefore, critical to predicting soil biogeochemical cycling and C fluxes.

The decomposition of soil organic matter is influenced not only by climatic variables, such as ecosystem temperature and moisture, but also by critical soil biogeochemical factors (Bradford et al. 2016). One such biogeochemical factor is the presence of redox-active metals, which can facilitate the oxidation of soil organic matter. Soil organic matter oxidation involves the depolymerization of larger organic compounds, such as particulate organic carbon (POC), into smaller, enzymatically accessible compounds and is a critical step in their decomposition (Meentemeyer 1978). Redox-active metals are effective at facilitating soil organic matter oxidation, and one such metal that has been demonstrated to play a critical role in soil organic matter oxidation in a multitude of ecosystems is manganese (Mn) (Berg et al. 2007; Keiluweit et al. 2015; Jones et al. 2018). However, few studies have quantified the impact of reactive

Mn species on decomposition as well as the underlying mechanisms that drive these processes.

Importance of Mn availability in soil environments

Mn availability has been demonstrated to be a critical factor in controlling decomposition and soil carbon storage. In over 4,500 forest soils across a wide climatic gradient in Sweden, increased Mn concentration was a stronger predictor for lower C storage (Stendahl et al. 2017) than any other climatic or edaphic variable, indicating the importance of Mn across a diverse array of environmental conditions. Additionally, litter incubation studies conducted in forests have demonstrated Mn to stimulate litter decomposition (Berg et al. 2007), and similar correlations have been demonstrated between Mn and soil CO_2 emissions in peatland systems (Dhandapani et al. 2021), further supporting the significant influence of Mn on decomposition and controlling C storage across ecosystems globally.

The role of Mn(III) and Mn availability

In soil environments, Mn is predominantly found in either Mn(II), Mn(III), or Mn(IV) oxidation states. Soluble Mn(II) can be enzymatically oxidized by microbes, particularly lignolytic fungi, to Mn(III) (Hofrichter 2002). Mn(III) is a highly reactive intermediate and potent oxidant that is effective at penetrating and depolymerizing large lignocellulose compounds such as wood, that enzymes are unable to access, and at enabling enzymatic decomposition (Hofrichter 2002). Enhanced Mn availability in fungal cultures increases Mn deposition on wood and has been implicated in enhancing wood degradation (Kirker et al. 2017; Pinzari et al. 2018). However, to what effect enhanced Mn availability has on microbially mediated Mn(III) formation and subsequent litter

decomposition remains unexplored. To date, only few Mn manipulation experiments have made explicit links between the amount of bioavailable Mn to the rate of organic matter oxidation, with most instead focused on Mn concentrations in soil and litter (Trum et al. 2015; Berg et al. 2015). In studies that do perform Mn manipulations, correlations made between Mn concentrations and litter decomposition show inconsistencies, such as undifferentiated aromaticity in dissolved organic carbon (DOC) with greater Mn additions despite enhancing decomposition rates (Trum et al. 2012; Trum et al. 2015). These discrepancies are difficult to resolve as an understanding of the underlying mechanisms that affect Mn–C coupled cycling are dependent on measuring Mn chemical transformations that are often not performed in litter incubations. Additionally, forest and agricultural litter incubations with Mn additions typically excluded the incorporation of redox dynamics (Sun et al. 2019), despite their importance in driving Mn transformations (Madison et al. 2013). The incorporation of critical components, such as redox dynamics involved in Mn–C coupled cycling studies, has been sparse, thereby limiting our understanding of the processes involved.

Mn redox cycling across oxic-anoxic interfaces

Manganese is subject to intense redox cycling in soils and sediments, which ultimately dictate their oxidation state across the redox gradient (Oldham et al. 2017; Hansel 2017). Mn speciation varies across redox gradients defined by gradually changing O_2 concentrations, which control the oxic and anoxic reactions involved in Mn cycling. In studies documenting Mn cycling in marine sediments, Mn oxides found along anoxic zones were reduced, which resulted in the mobilization and translocation of Mn(II) across the oxic-anoxic interface (OAI) to then allow Mn(III) formation (Trouwborst et al. 2006;

Madison et al. 2013; Oldham et al. 2017; Jones and Tebo 2021). Subsequently, Mn(III) formation at OAIs can then facilitate POC oxidation (Jones et al. 2018) and play a major role in Mn–C coupled cycling across redox gradients. In anoxic zones, the reduction of Mn oxides can be facilitated microbially when conditions are energetically favorable for Mn respiration coupled to organic matter degradation (Tebo 1991; Warrinnier et al. 2020; LaRowe et al. 2021). In addition, the abiotic oxidation of POC via Mn oxide-catalyzed reactions has been demonstrated to be a major factor in Mn–C coupled cycling (Ma et al. 2020) and has been implicated in tropical forest systems (Sanchez et al. 2021), indicating both biotic and abiotic processes are critical in anoxic environments. These interactions show that Mn transformations and the formation of reactive Mn(III) is controlled by both biotic and abiotic processes, but the individual contributions of each process to Mn–C coupled cycling are largely unknown.

Mn(III)-mediated C oxidation at oxic-anoxic interfaces

In soil systems, Mn(III) formation is primarily facilitated by the microbial oxidation of Mn(II), particularly by lignolytic fungi that produce enzymes such as manganese peroxidase (Hofrichter 2002; Zeiner et al. 2016). Soil incubations studies have shown fungal-mediated Mn oxidation occurring at OAIs (Thompson et al. 2005), indicating that microbial processes are critical for Mn cycling in soils. The absence of fungi that facilitate Mn transformations has been demonstrated to weaken the effect of Mn concentrations on organic matter degradation (Kranabetter 2019), emphasizing microbial Mn oxidation as a constraint on POC oxidation. A recent study conducted by Jones et al. (2018) using incubations of forest soils within diffusion reactors with a fixed redox gradient showed that overlapping Mn and O_2 gradients resulted in measurable Mn

oxidation and POC oxidation at the OAI (Jones et al. 2018). Additionally, this study also found the highest potential for POC oxidation at the OAI and indicated that the incorporation of redox gradients is critical for understanding soil Mn cycling. In summary, it is clear that Mn bioavailability and microbially mediated Mn(III) formation at OAIs are critical components involved in POC oxidation. However, while the significance of Mn bioavailability and its impact on soil C decomposition is increasingly being recognized (Keiluweit et al. 2015; Li et al. 2021), its effect on POC oxidation along redox gradients has yet to be examined in spite of overwhelming evidence of its impact in ecosystem studies (Trum et al. 2015; Berg et al. 2015; Stendahl et al. 2017; Sun et al. 2019).

Current knowledge gap in understanding Mn–C coupled cycling across redox gradients

While Jones et al. (2018) were able to show Mn-mediated POC oxidation at OAIs, they were unable to elucidate the importance of different abiotically and microbially driven Mn transformations across the redox gradient. Jones et al. (2018) were also unable to determine the role of biotic and abiotic Mn reduction coupled with POC oxidation in anoxic zones driving Mn mobilization—a significant knowledge gap in Mn cycling in soil environments. Finally, Jones et al. (2018) did not quantify how Mn redox cycling across the redox gradient affects CO_2 production and the relative contributions of abiotic and biotic Mn reactions to POC oxidation. Specifically, the contributions of microbial and abiotic Mn(II) oxidation coupled with POC oxidation at OAIs (Hofrichter 2002; Madison et al. 2013; Oldham et al. 2017), and anoxic Mn oxide reduction coupled with both abiotic POC oxidation (Ma et al. 2020) and microbial respiration (LaRowe et al. 2021) were not explored and are a significant unknown in understanding Mn–C

coupled cycling across redox gradients.

Our study aimed to quantify the impact of Mn availability on Mn-mediated POC oxidation across the redox gradient and the specific contributions of abiotic and biotic reactions. To do this, we varied Mn availability along redox gradients established within soil diffusion reactors and assessed the corresponding changes in POC oxidation across the redox gradient. Diffusion reactors designed to establish a stable redox gradient were packed with varying Mn concentrations and POC (oak chips), and then incubated for 90 days. Placement of Mn oxides of various amounts within the anoxic zone of the reactors allowed us to manipulate Mn(II) translocation across the OAI. All reactors were amended with microbial inoculum except for uninoculated controls, which were conducted to decipher the relative importance of abiotic and biotic processes. Changes in Mn oxidation state along the redox gradient was determined using a combination of wet-chemical extractions and X-ray absorption near edge structure (XANES) spectroscopy. The impact on POC oxidation was determined using a combination of C near edge X-ray absorption fine structure (NEXAFS) spectroscopy and continuous CO_2 measurements. This experimental design allowed us to examine the abiotic and biotic contributions to (i) Mn reduction to supplying Mn(II) from the anoxic zone towards the OAI, (ii) Mn oxide-driven POC oxidation in the anoxic zone, and (iii) Mn(III)-mediated POC oxidation at the OAI.

Figure 1 and **Table 1** display the primary reactions investigated in our study as well as the hypothesized outcomes in our reactor treatments:

1) We hypothesized that enhanced Mn availability would increase the amount of Mn(II) mobilized via reductive dissolution, especially in our inoculated

treatment. We expected a subsequent increase in Mn(III) formation at the OAI, which would lead to enhanced POC oxidation and CO_2 production (Figure 1b).

2) Additionally, we hypothesized that uninoculated treatments would show lower Mn oxide-catalyzed C oxidation in the anoxic zone (Table 1.III) and Mn(III)-mediated C oxidation at the OAI (Table 1.I) compared with inoculated treatments (Figure 1c). Conversely, the inoculated treatment was expected to show greater C oxidation due to enhanced microbial Mn oxide reduction (Table 1.IV) and Mn(III)-mediated POC oxidation at the OAI (Table 1.II).

Our overall work quantifies the relative importance of microbial and abiotic processes in controlling Mn translocation and reactive Mn formation along redox gradients.

CHAPTER 2

METHODS

2.1 Diffusion Reactors

To establish a stable redox gradient that we could utilize to measure Mn transformations, we used proven diffusion reactors adopted from Jones et al. (2018). Reactors were made of a polycarbonate case (10 x 8 x 1 cm) with openings at the top to allow oxygen to diffuse into the soil matrix. An inlet at the bottom of the reactor allowed us to regulate the water table height and control the position of the OAI.

To reduce interference with other redox sensitive elements like iron (Fe), we created an artificial soil consisting of sand, oak chips, and microbial inoculum. Sand (Fisher Scientific, Hampton, NH) was washed three times by acid washing with 0.5 M HCl to remove residual metals and then rinsed with nanopure water before drying. The Mn manipulations were provided via the synthesis of acid birnessite (Villalobos et al. 2003), which allowed for the dissolution and mobilization of Mn under anoxic conditions across the redox gradient. Mn treatments were established by coating the washed sands with designated concentrations on a mass-by-mass basis using an acid birnessite slurry mixed into the sand that was allowed to dry over 96 hours. Oak chips were used as a proxy for POC and were oven dried at 105°C for 24 hours prior to the start of the experiment to minimize microbial activity.

To determine the influence of Mn availability on Mn cycling across the redox gradient, we established three inoculated Mn treatments of varying concentrations (control – 0 μg/g Mn; low-Mn – 400 μg/g Mn; high-Mn – 2000 μg/g Mn). The selected Mn treatments spanned a range of Mn concentrations observed in studies of forest litter

and soil horizons (Blume et al. 2015; Berg et al. 2015). An additional uninoculated treatment (no inoculum treatment –2000 μg/g Mn) allowed us to quantify abiotic Mn oxide-catalyzed and Mn(III)-mediated POC oxidation. Soil inoculum was extracted using 1200 mL of an artificial soil solution on a mixture of 10% litter, 80% O-horizon, and 10% A-horizon soil collected at Harvard Forest during the Summer (Harvard Forest, Petersham, MA). The artificial soil solution consisted of a nutrient solution premade to mimic Harvard Forest groundwater concentrations for our sampling site (Table S-1). A 20 mm Mn oxides layer at the bottom of the reactor was established in the Mn treatments as follows: 36g of sand and oak chips (1:100 ratio) received 41 mL of microbial inoculate (excluding the no inoculum treatment) and packed at the bottom 20 mm of the reactors. The upper 35 mm of all reactors were then packed with 54 g of sand-oak chip mixture (1:100) and in inoculated treatments were amended with 61 mL of microbial inoculum. The non-inoculated treatments received equivalent volumes of sterile artificial soil solution. Reactors were then wetted through the inlet with our artificial soil solution to establish the water table at 12–18 mm below the soil surface for the duration of the experiment. Triplicate reactors were incubated in the dark at 23 °C and then harvested after 90 days.

2.2 Reactor Sampling

Reactors were harvested at 90 days in an anoxic atmosphere (97%/3% N_2/H_2) within an anaerobic chamber (Coy Laboratory Products Inc., Ann Arbor, MI) to minimize changes to sample oxidation due to atmospheric exposure. The soil profile was divided into four subsections designated oxic (0–12 mm), interface (12–18 mm), anoxic bulk (18–35 mm), and anoxic Mn layer (35–55 mm) that were sampled accordingly.

Reactor samples were drained of liquid first and then the inlet using syringes, removed from the anaerobic chamber and frozen, and then freeze-dried using a lyophilizer (Labconco, Kansas City, MO) for 72 hours before being stored in an anaerobic chamber until further processing.

2.3 Sequential Extractions

Reactive Mn phases and total abundance of Mn phases of different crystallinity were determined using pyrophosphate extractions and sequential extractions, respectively, following a similar protocol adopted from Jones et al. (2020). Sequential extractions were done using a sequence of H_2O, hydroxylamine, and dithionite-HCl as the extractants. Extracts were analyzed on an MP-AES (Agilent Technologies, Santa Clara, CA). We similarly measured Fe to account for potential contributions from Fe-C coupled redox reactions. To estimate POC associated with the various Mn phases, we used a total organic carbon analyzer (Shimadzu TOC-L) to measure water-extractable organic carbon (WEOC) in both the H_2O extracts and the pyrophosphate extracts.

2.4 CO_2 Measurements

CO_2 measurements were conducted throughout the experiment to quantify differences in CO_2 production due to treatment effects. Briefly, to quantify CO_2 production over time, openings on top of the reactors were sealed with silicon stoppers for 6 hours to allow the reactors to accumulate CO_2. CO_2 was sampled through septa and quantified on an infrared gas analyzer (LI-COR Biosciences LI-8100A, Lincoln, NE). Measured concentrations were used to calculate cumulative respiration over the course of the experiment. Sealants were then removed after measurement. Gas sampling occurred

between 2–3-day intervals for the first 30 days of the experiment, and afterwards was measured with decreasing frequency up until the end of the experiment.

2.5 Manganese XANES and Carbon NEXAFS Spectroscopy

To determine average Mn oxidation, reactor samples were analyzed using Mn K-edge XANES at the soft x-ray micro-characterization beamline (SXRMB) at the Canadian Light Source (Saskatoon, Saskatchewan, Canada). Triplicate samples were ground, homogenized, and combined before being mounted on a sample holder with carbon tape. Linear combination fitting in Athena under the Demeter package was used to quantify the relative abundance of Mn(II), Mn(III), and Mn(IV) and to determine the average Mn oxidation state (Ravel and Newville 2005; Manceau et al. 2012).

Changes in C oxidation state and functional groups were determined using C K-edge NEXAFS at the spherical grating monochromator beamline at the Canadian Light Source. Analyzed data were processed using the Athena software through peak fitting, with key functional groups and parameters (Table S-2) adopted from Keiluweit et al. (2017)**.** Changes in POC characterization were integrated with Mn chemistry to determine Mn-driven POC oxidation throughout the reactor profile.

2.6 Statistics

Comparisons for CO_2 production between treatments were done using model comparisons between respiration data fitted to a single first-order kinetic model (Tian et al. 1992; Sleutel et al. 2005). Statistical comparisons were done using an F-test comparison for fitted models and the results are displayed in Table S-5. Statistical comparisons were done for sequential extractions using a 1-way ANOVA Tukey test for

comparisons between corresponding sampling layers and extractants between treatments. Individual P-values between comparisons are given in Table S-4.

CHAPTER 3

RESULTS

3.1 Mn sequential extractions and XANES

Wet chemical extractions combined with Mn XANES showed enhanced Mn availability with increased initial Mn concentrations in inoculated reactors (Figure 2). The highest extractable Mn from the reactor matrix was found in the high-Mn treatment, followed by the low-Mn treatment, the uninoculated high-Mn treatment, and no-Mn treatment. Across both the low and high-Mn treatments, the greatest quantity of oxidized Mn, barring the treatment zone, was found at the OAI (12–18 mm). At the OAI, the high-Mn and low-Mn treatments had 19x and 13x higher extractable Mn, respectively, than the uninoculated treatment. Hydroxylamine extractions accounted for 40–60% of the total Mn in both the low and high-Mn treatments within the 0–12, 12–18, and 18–35 mm sampling zones. Within the no inoculum treatment, hydroxylamine extractable Mn contributed between 60–80% of the sampling zones. While dithionite-extractable Mn represented between 70–85% of the total Mn in the control treatment, it only represented approximately 3% of the total Mn in our Mn-amended treatments. Extractable Mn increased with Mn availability in both our high and low Mn treatment but not our no inoculum treatment relative to the control treatment (Figure S-1, Table S-4).

Mn XANES estimates of the relative contribution of Mn valence states showed higher Mn(III) in the high-Mn treatment compared with the low-Mn treatment (Figure 2). Total Mn(III) was 2-3x greater in the high-Mn treatment within the OAI sampling zone compared with the low-Mn treatment. Total extractable oxidized Mn (Mn(III) + Mn(IV)) was greatest in the high-Mn treatment, followed by the low-Mn, then the no inoculum

treatment, and finally the control treatments. Overall, Mn analysis showed enhanced Mn availability under inoculated treatments resulted in higher Mn translocated to the upper depths of the reactor matrix and an increase in total oxidized Mn.

3.2 CO_2 Production

Enhanced Mn availability and microbial inoculum significantly increased CO_2 in our experiments. Over the 90-day incubation period, cumulative CO_2 measurements of our incubated soil reactor (Figure 3) showed that both the high and low-Mn treatments had greater CO_2 production than the no inoculum treatment by 55% and 32%, respectively. The high-Mn treatment CO_2 production was statistically greater than all other treatments ($P < 0.01$) (Table S-5). CO_2 measured in the high-Mn treatment was also 25% greater than the control treatment, while cumulative CO_2 measured in the low-Mn treatment was 1% lower than the control treatments after 90 days. Additionally, CO_2 measured in the high and low Mn treatments were 48% and 33% higher than the no inoculum treatment after 14 days and were also 25% and 12% higher than the control treatment, respectively. While the low-Mn and control treatment were not statistically different from each other ($P = 0.12$), both were greater than the no inoculum treatment ($P<0.01$). Overall, the high-Mn treatment had the greatest CO_2 measurement for cumulative CO_2, while the low-Mn treatment showed greater CO_2 production than both the no inoculum and control treatments only during the first two weeks of CO_2 sampling.

3.3 C NEXAFS and Characterization

C NEXAFS spectroscopy conducted on our bulk samples showed increasing POC oxidation with increasing Mn availability. A list of specific functional groups analyzed and their relative contribution to POC chemistry is included in Table S-3. In particular,

the ratio between Carboxylic:Aromatic peaks is a measure of the degree of oxidation of POC, with higher ratios indicative of increased POC oxidation. The high-Mn treatment has the greatest Carboxylic:Aromatic peak ratio at the redox interface, which declines with depth (Figure 4). Additional changes in C functional groups (Table S-3) showed the greatest decrease in C groups associated with aromaticity (Quinone, Aromatic, and Phenolic) at the high-Mn OAI sampling zone compared with all other treatments (Table S-6). Measurements in both Mn Oxide treatment layer and the OAI in the high-Mn treatment indicate greater POC oxidation than the no inoculum treatment, likely attributed to microbial oxidation (Figure 4, Figure S-6, Table S-3). Overall, C NEXAFS showed greater OM oxidation across the high-Mn treatment compared to the no inoculum treatment.

CHAPTER 4

DISCUSSION

Our experimental results showed that POC oxidation was driven by enhanced Mn cycling along the redox gradient. Increasing Mn oxide concentrations enhanced Mn(II) translocation to the OAI. Increased Mn(II) availability at the redox interface resulted in increased Mn(II) oxidation and Mn(III) formation at the OAI, which subsequently increased POC oxidation and CO_2 production. With inhibited microbial activity (no inoculum treatment), Mn oxide reduction and Mn(II) translocation across the redox gradients decreased, resulting in decreased Mn oxidation at the OAI. This reduced Mn redox cycling across the redox gradient in the no inoculum treatment resulted in lower POC oxidation and CO_2 production. Comparison of the inoculated and uninoculated treatments further suggests that enhanced POC oxidation was principally facilitated by complex Mn(III)-driven reactions, rather than Mn oxide-catalyzed POC oxidation alone. Overall, our experimental results show strong links between the Mn(II) supply through microbial Mn oxide reduction, Mn(III) oxidation, and POC degradation across the gradient, highlighting the critical role of microbial Mn cycling in C oxidation within redox-active soils and sediments.

4.1 Enhanced Mn availability increases Mn cycling across the redox gradient

Enhanced Mn concentrations and the incorporation of microbial processes (both reduction and oxidation across the OAI) enhanced Mn cycling across the redox gradient. Increasing Mn translocation with increasing Mn concentration, especially in the high-Mn treatment, resulted in both higher total and reactive Mn formation at the OAI. The increased reactive Mn formation suggests that the addition of Mn oxides enhanced the

total Mn translocated via anoxic reduction, which increased the supply of Mn(II) at the OAI for both abiotic and biotic oxidation. This is indicated by the increasing concentration and presence of oxidized Mn, which was observed in both Mn extractions as well as solid phase characterization of the Mn oxidation state in our reactors (Figure 2).

Interestingly, we did not notice a distinct band of Mn oxide formation that has been observed in other soil Mn incubation experiments in conjunction with increased reactive Mn formation (Thompson et al. 2005; Jones et al. 2018). There are several possible reasons for this, with one of them being that Mn(III) quantification is difficult as its sensitive and transient nature makes it difficult to detect and distinguish from dissolved Mn(II) (Kim et al. 2022). Additionally, the lack of Mn-oxidizing microbes in our inoculum (Zelinka et al. 2021) may have limited Mn oxidation at the OAI. The inoculum likely favored bacteria over fungi (Kallenbach et al. 2016), which are known to facilitate Mn oxidation at OAIs (Thompson et al. 2015), highlighting the need for further study of the Mn-oxidizing microbes in forest soils. Additionally, Mn oxide formation can be inhibited by several soil conditions, including ligand concentration, pH, and rapid interaction between Mn(III) and POC (Duckworth and Sposito 2005; Morgan et al. 2021). Mn influences on POC oxidation is also a time-dependent process, and the activity of different species of fungi facilitating Mn oxidation has been shown to be highly variable as well (Perez and Jeffries 1992; Zeiner et al. 2016; Yue et al. 2021), suggesting that we possibly did not run the incubation long enough for our specific system. In contrast, it is also possible that the 90-day duration of our experiment exceeded the optimal time for Mn band formation that have been observed after 30 days (Jones et al.

2018). The extended incubation period may have allowed the Mn band to be chemically diffused through microbial reduction (Stone 1987), thereby dissipating the observable band. The numerous factors involved in Mn oxide formation and dissolution at OAIs point to their sensitivity and indicate a need for further investigation into understanding the temporal dynamics involved in the formation of Mn(III) and Mn transformations across redox gradients.

4.2 Abiotic Mn reduction plays a minor role in mobilizing Mn across the redox gradient

By isolating the impacts of abiotic processes on Mn–C coupled cycling across the redox gradient, we were able to determine that abiotic processes play a minor contribution in mobilizing Mn and subsequent reductions in Mn oxidation at the OAI compared with inoculated treatments. Having primarily abiotic reduction of Mn oxide in the anoxic layers resulted in a decrease in Mn mobilized across the redox gradient compared to inoculated treatments, leading to less Mn formation at the OAI due to lower Mn and slower oxidation kinetics (Gregory and Carlson 2003). We observed a decrease in total reactive Mn(III) at the interface in the no inoculum treatment compared with the high Mn treatment, which indicates that the removal of microbial processes occurring both anoxically and at the OAI reduces the supply of Mn translocated to the OAI, stifling reactive Mn(III) formation. Our observations can be explained by studies comparing the reduction rates of different Mn minerals by microbes and abiotic mechanisms in which bacterial reduction tends to be more rapid (Johnson et al. 2016), although these outcomes may be dependent on the types of Mn minerals and chemical conditions present in the environment (Burdige et al. 2009). Additionally, the diverse mechanisms of bacteria with respect to the chemical alteration of mineral surfaces and chemical environments allow

thermodynamic limitations found in abiotic Mn dissolution to be overcome (Luther and Popp 2002; Burdige et al. 2009), which may explain the enhanced Mn reduction found in our high-Mn reactors compared with our no inoculum treatment. Overall, our findings emphasize the importance of microbial processes, particularly the anaerobic Mn respiration and subsequent Mn reduction, in mobilizing Mn(II) and controlling the flow of Mn(II) throughout Mn–C coupled cycling.

4.3 Enhanced Mn availability increases microbial Mn(III)-mediated POC oxidation at OAIs, but not abiotic Mn oxide-catalyzed POC oxidation

Enhancing Mn oxide concentrations led to an increase in the formation of reactive Mn at OAIs, which subsequently enhanced Mn(III)-mediated POC oxidation while having minimal impact on Mn oxide-catalyzed POC oxidation. At the anoxic layer, the C NEXAFS spectra (Figure 4) suggests that there were little differences between the high-Mn and no inoculum treatment, indicating that anoxic POC oxidation was largely unaffected by the addition of anaerobic microbes. Further characterization of water extractable organic carbon also indicated little differences between the no inoculum treatment and the inoculated Mn treatments (Figure S-2). This may have been due to increasing Mn concentrations in anoxic zones during Mn oxide reduction (Oldham et al. 2017), which negatively impact the predominantly bacterial communities in anoxic environments (Reith et al. 2002) that can be more sensitive to metal toxicity and leads to decreased overall activity (Hiroki 2012). Increasing Mn oxide concentrations does, however, increase the mobilization of Mn(II) to the OAI, which subsequently promotes microbial Mn(II) oxidation at OAIs (Madison et al. 2013; Whalen et al. 2018) and likely results in enhanced Mn(III) formation, Mn(III)-mediated POC oxidation, and CO_2

production (Jones et al. 2018). This was best demonstrated by the differences between our control and high-Mn treatments in which the resulting increase in both Mn availability and reactive Mn formation at the OAI resulted in greater POC oxidation and subsequent CO_2 production in the high-Mn reactors. An increase in carboxylic groups in POC found at the OAI suggests the oxidation of aromatic compounds (Figure 4, Figure 5, Table S-3, Table S-6) (Hofrichter 2002), and reinforces that the process was driven by enhanced Mn availability. Additionally, Mn was likely the primary driver of POC oxidation as Fe analysis revealed no differences among the inoculated reactor treatments (Figure S-7). Therefore, we can see that Mn(III)-mediated POC oxidation is driven primarily by the increased translocation of Mn to the OAI. Mn(III) formation at the OAI is primarily microbially driven, resulting in the greatest impact in our high-Mn treatment. Total carbon analysis in the anoxic zones showed similar concentrations of total organic carbon between the high-Mn and no inoculum treatment, suggesting that microbes are unable to utilize the dissolved organic carbon (DOC) resulting from depolymerized POC (Figure S-3). While our study did not explicitly measure DOC respiration, we would expect that enhanced POC oxidation and subsequently greater DOC concentrations would lead to increased CO_2 (Bengtson and Bengtsson 2007); our findings suggest that other mechanisms may be responsible for inhibiting DOC respiration. Therefore, this aspect of Mn–C coupled cycling requires further studying to understand the complexities between POC oxidation and complete decomposition to CO_2.

Contrary to our hypothesis that enhanced Mn availability would directly lead to enhanced POC oxidation, the low-Mn treatment demonstrates that this is not necessarily the case. When comparing the low-Mn treatment respiration to our control treatment,

there were only minor differences in CO_2 (Figure 3). This suggests the possibility that Mn availability and its impact on POC oxidation may be affected by thresholds, and that Mn itself in low quantities may be impeding POC degradation due to either effects of microbial toxicity or inhibiting substrate access through mineral binding. Examples of aquatic Mn oxidizers being inhibited by low Mn(II) concentrations support the possibility that the low-Mn treatment may have been toxic to microbes, thereby impacting reactive Mn formation and subsequent POC oxidation at OAIs (Chapnick et al. 1982). While observations of Mn inhibiting Mn–oxidizing enzymes and subsequently POC degradation have been shown (Kranabetter 2019), the reasoning behind what threshold determines when Mn concentrations have more of a promotional rather than inhibitory effect on POC oxidation have not been explored. One possible explanation may be that the effects of differing metal concentrations vary depending on the microbial communities present, as observed in studies on other redox-active metal ions such as copper that demonstrated reduced bacterial activity high metal concentrations while fungal activity was enhanced (Rajapaksha et al. 2004). It is possible that specific concentrations of Mn have opposite interactions between bacteria and fungi in our reactors, given that fungi are more resilient to high metal concentrations (Hiroki 2012), which inhibited the overall microbial respiration in the low-Mn treatment.

4.4 Mn oxide-catalyzed POC oxidation plays a critical role in Mn-C coupled cycling

POC oxidation inferred through C NEXAFS were similar between our high-Mn and no inoculum treatment. This would indicate that Mn oxide catalyzed POC oxidation was the primary driver, and contributions from anaerobic Mn respiration was minor (Figure 4, Figure S-4). This is possibly due to unfavorable energetics or the presence of

other electron acceptors like NO_3^-, making specific metabolisms like Mn respiration unfavorable in our system (Nealson and Myers 1992) despite the observation that increased microbial presence enhanced Mn reduction and mobilization (Figure 2). Another possibility includes Mn toxicity leading to decreased bacterial activity (Chapnick et al. 1982; Hiroki 2012). The lower Mn mobilization in the no inoculum treatment, however, resulted in reduced Mn-driven POC oxidation at the OAI, limiting POC oxidation and leading to a lower measured CO_2 response in the no inoculum treatment compared with the high-Mn treatment (Figure 2, Figure 3). However, it is important to note that the processes at the OAI are dependent on Mn mobilization, which was highly dependent on the anoxic reduction of Mn oxides facilitated by microbes in our reactors (Madison et al. 2013; Jones et al. 2018). These processes not only emphasize the significance of both abiotic and biotic processes in driving Mn–C coupled cycling across redox gradients, but also their interdependence. Additionally, the no inoculum treatment total CO_2 production accounted for nearly 60% of that measured in the high-Mn treatment, which implies that the abiotic contribution to POC oxidation was significant but did not fully account for the increase in the high-Mn treatment, thereby emphasizing the importance of microbial processes in Mn–C cycling. Our findings in their entirety indicate that Mn availability is a significant factor in driving Mn-mediated POC oxidation but is highly dependent on Mn–C coupled reactions occurring across the redox gradient.

CHAPTER 5

CONCLUSION

Mn cycling plays a significant role in litter decomposition, particularly in many forested ecosystems (Berg et al. 2007; Keiluweit et al. 2015; Trum et al. 2015). In forest systems, Mn-mediated litter decomposition is thought to be governed by the formation of reactive Mn(III) (Keiluweit et al. 2015; Li et al. 2021), which in turn is dependent on the presence of redox gradients (Madison et al. 2013; Jones et al. 2018). Our results reinforce the significance of microbially-driven Mn(III)-mediated POC oxidation at OAIs and emphasize the dependency of Mn(III) formation on anaerobic microbial Mn reduction. Mn reduction under anoxic conditions is a critical step in mobilizing Mn(II) to OAIs and, given the ubiquity of anoxic microsites in soils (Van Der Lee et al. 1999; Keiluweit et al. 2017), represents an unappreciated catalyst for organic matter decomposition. These effects are further enhanced by increasing Mn concentrations, which have been noted to occur in both litter and mineral soil (Aponte et al. 2012; Rennert et al. 2014), and have been impacted by anthropogenic activity and deposition (Herndon et al. 2011). Our incorporation of redox dynamics shows that increasing Mn bioavailability enhances POC oxidation to an extent, but Mn bioavailability is ultimately dictated by processes along redox gradients, particularly Mn(II) mobilization via anoxic Mn reduction. These findings emphasize the need to incorporate redox dynamics when assessing the impact of Mn concentrations on litter decomposition rates that are often unaccounted for in Mn field studies. Combined, our results point to the high potential impact that Mn–C coupled cycling across redox gradients have on organic matter decomposition and, ultimately, CO_2 production. Redox gradients and OAIs are increasingly recognized as important

zones of microbial and chemical activity, leading to hotspots of enhanced POC oxidation. Redox-active metals such as Mn are actively utilized and cycled as instruments for organic matter oxidation, and the microenvironments in which they exist dictate their utilization in decomposition. The spatial and temporal dynamics involved in their biogeochemical transformations have profound impacts on organic matter decomposition, and improving our understanding of critical biogeochemical processes, such as Mn redox cycling, will be critical for accurate predictions of climate change impacts on soil C storage and CO_2 fluxes.

APPENDIX

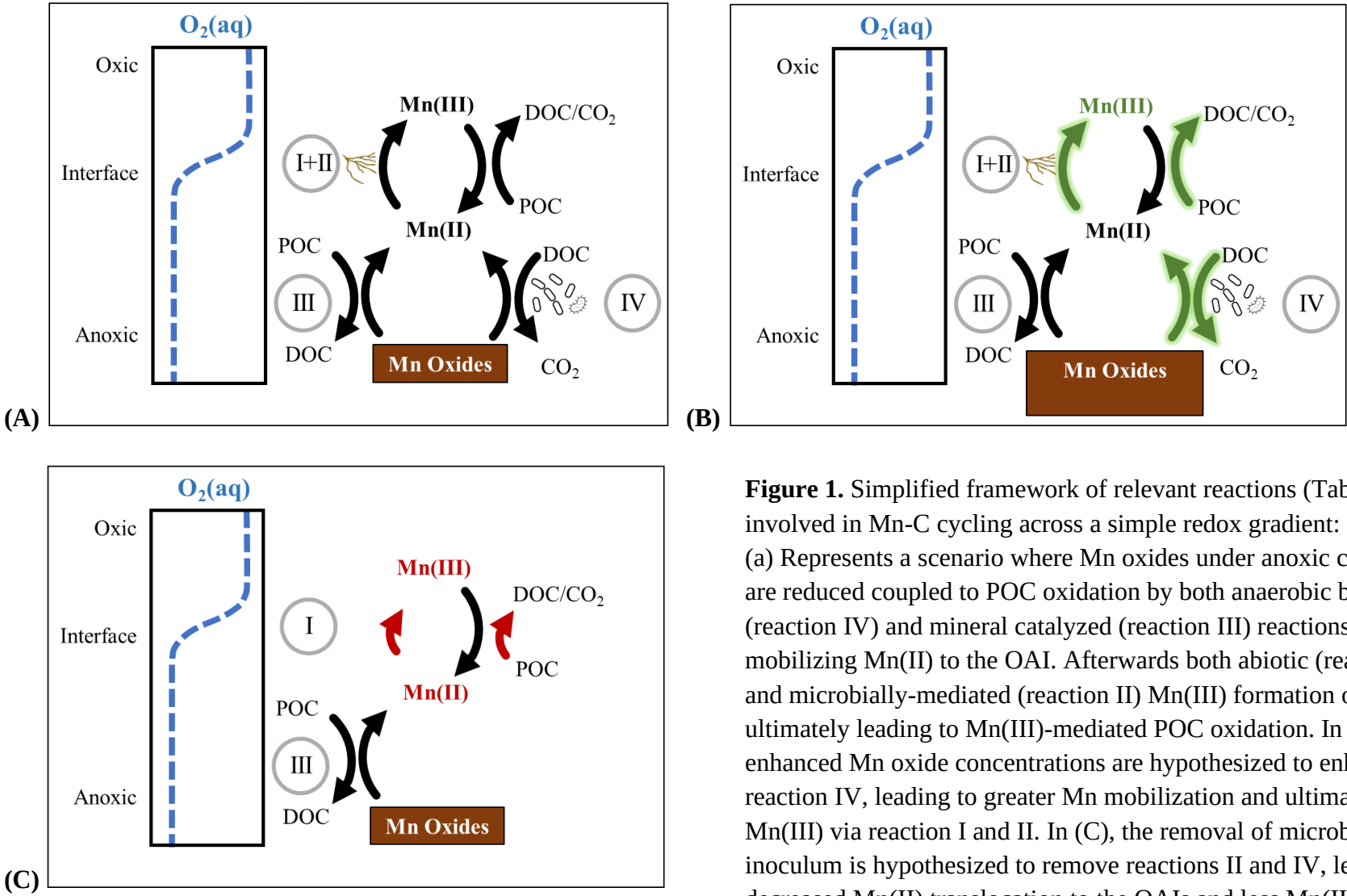

Figure 1. Simplified framework of relevant reactions (Table 1) involved in Mn-C cycling across a simple redox gradient: (a) Represents a scenario where Mn oxides under anoxic conditions are reduced coupled to POC oxidation by both anaerobic bacteria (reaction IV) and mineral catalyzed (reaction III) reactions, mobilizing Mn(II) to the OAI. Afterwards both abiotic (reaction I) and microbially-mediated (reaction II) Mn(III) formation occurs, ultimately leading to Mn(III)-mediated POC oxidation. In (b) enhanced Mn oxide concentrations are hypothesized to enhance reaction IV, leading to greater Mn mobilization and ultimately Mn(III) via reaction I and II. In (C), the removal of microbial inoculum is hypothesized to remove reactions II and IV, leading to decreased Mn(II) translocation to the OAIs and less Mn(III) formation and Mn(III)-mediated POC oxidation.

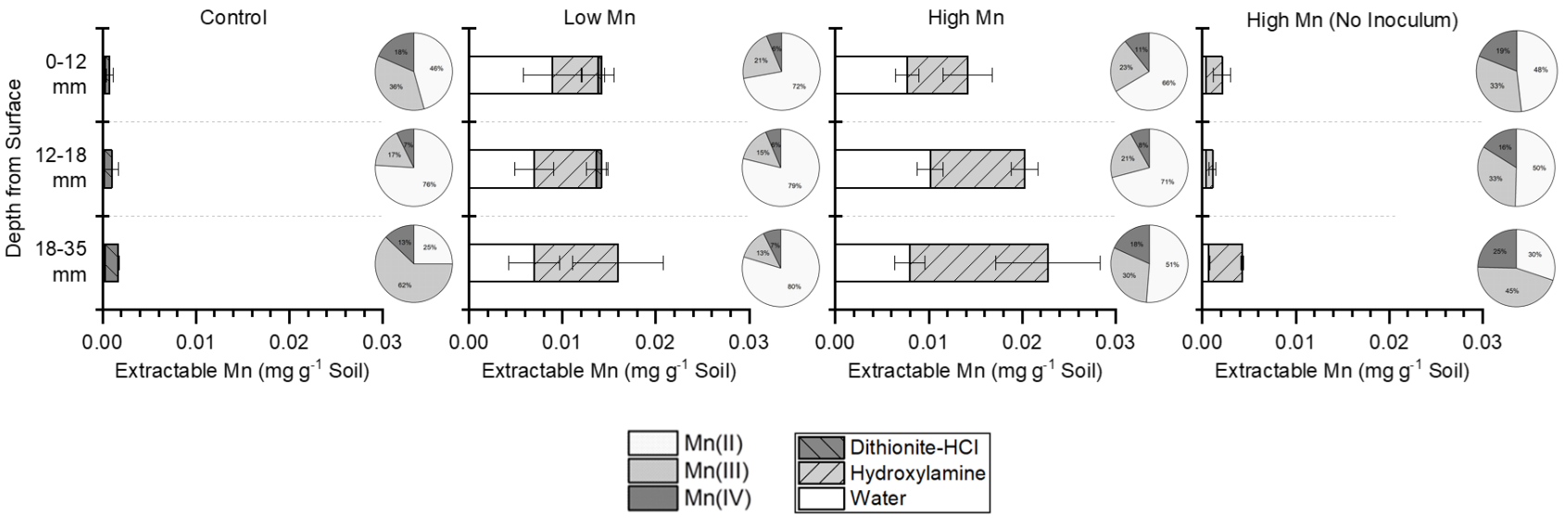

Figure 2 Change in Mn concentration across the redox gradient for our reactor treatments. Bar graphs denote Mn extracted by sequential dissolution using water, hydroxylamine, and dithionite-HCl. Pier charts show the relative contribution of Mn(II),(III), and (IV)

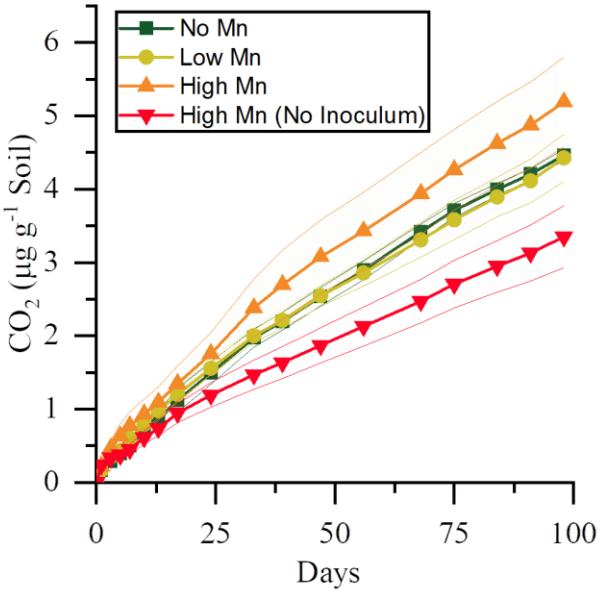

Figure 3. Effects of Mn availability and inoculation on cumulative CO_2 production. Error bars denote standard error of the mean (n=3).

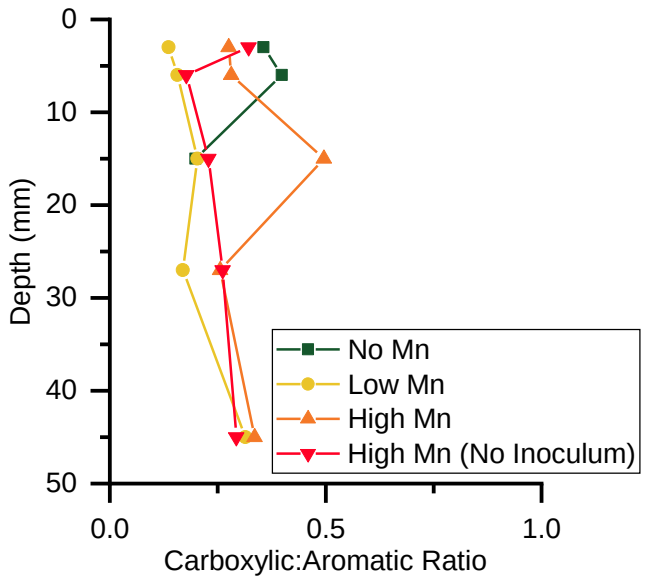

Figure 4. Change in C functional group (carboxylic and aromatic) across the redox gradient under different Mn treated reactors conducted on solid-phase samples collected at the end of the incubation period. Values determined by utilizing peak fitting using a method from (Keiluweit et al. 2017, Solomon et al. 2007) and focused on the carboxylic and aromatic peaks – ratio is a proxy for the oxidation of C compounds.

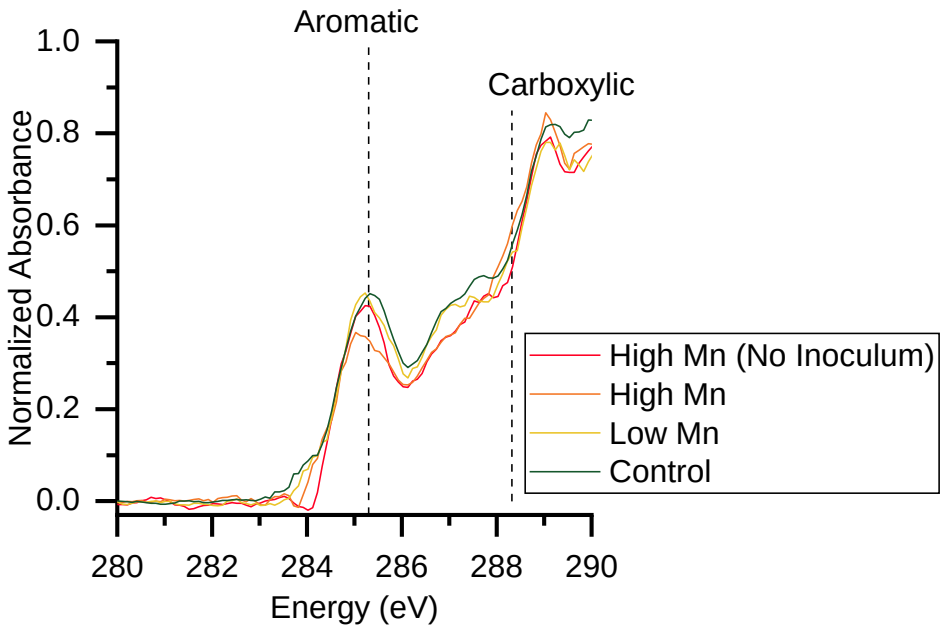

Figure 5. C NEXAFS spectra corresponding to the 12-18 mm depth transition layer. Two peaks of interest are selected – aromatic (285.3 eV ± 0.5 width) and carboxylic (288.3 eV ± 0.5 eV).

Table 1. Hypothesized and simplified primary reactions (unbalanced) involved in abiotic and biotic Mn cycling across redox gradients. In reaction I, abiotic oxidation of Mn(II) via reactive oxygen species (reaction Ia) allow for the formation of Mn(III), which subsequently oxidizes POC (reaction Ib). In reaction II, microbial enzymes like MnP facilitate the formation of Mn(III) which is subsequently stabilized in solution by ligands (reaction IIa) before participating in POC oxidation (reaction IIb). Reactions III and IV represent anoxic processes – reaction III represents Mn oxide-surface catalyzed oxidation of POC, while reaction IV is an example of Mn respiration performed by anaerobic microbes.

Redox Condition	Pathway	Reaction No.	Abiotic or Biotic	Chemical Reaction	Refs
Oxic	Mn(III) formation and subsequent Mn(III)-mediated C oxidation	I	Abiotic	a) Abiotic Mn oxidation: $Mn(II) + O_2^- + 2H^+ \xrightarrow{L} Mn(III) - L + H_2O_2$ b) Mn reduction coupled to C oxidation: Mn(III)-L + POC → DOC + Mn(II)	(Madison et al. 2013; Oldham et al. 2017b)
		II	Biotic	a) Microbially mediated Mn oxidation: $H_2O_2 + 2\,Mn(II) \xrightarrow{MnP} 2Mn(III) + H_2O$ b) Mn reduction coupled to C oxidation: Mn(III)-L + POC → DOC + Mn(II)	(Hofrichter 2002)
Anoxic	Mn Oxide catalyzed POC oxidation	III	Abiotic	$Mn(IV)O_x + POC \rightarrow Mn(II) + DOC$ $CH_2O + MnO_2 \xrightarrow{L} Mn(III)\text{-}L + CO_2 + H_2O$	(Madison et al. 2013; Ma et al. 2020)
	Anaerobic Mn respiration	IV	Biotic	$MnO_2 + C_vH_wO_xN_yP_z + H^+ \rightarrow N_2 + HCO_3^- + HPO_4^{2-} + Mn^{2+} + H_2O$	(Froelich et al. 1979)

Supplementary Information:

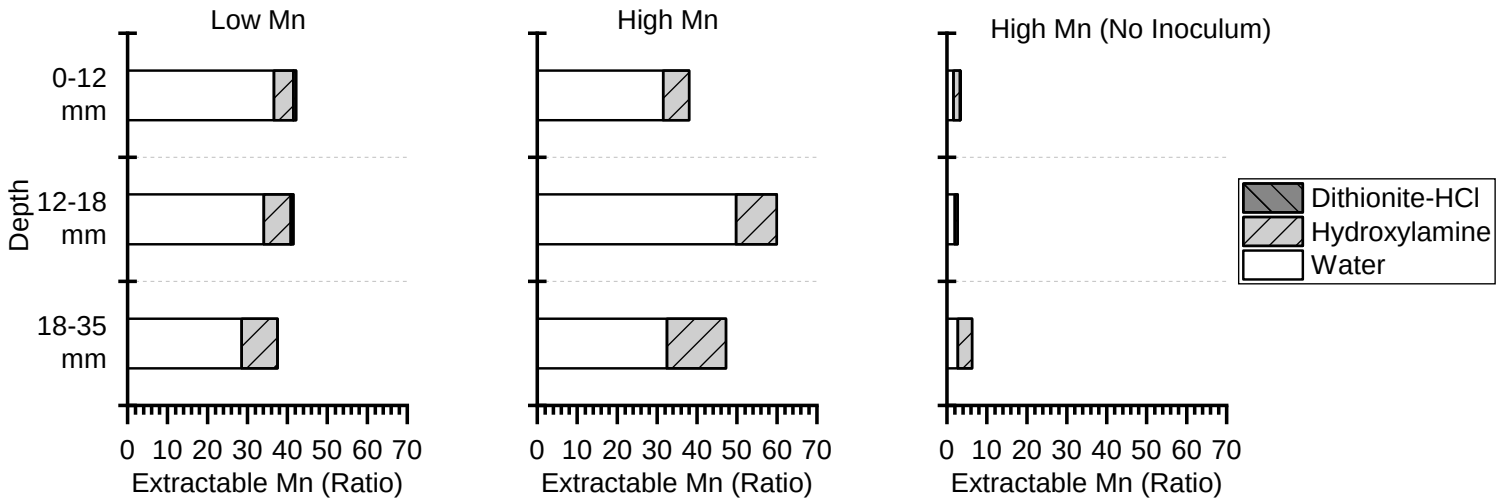

S.I. Figure 1. Mn sequential extractions normalized to the Control treatment extraction pools, where the X-axis is a representation of the ratio to control.

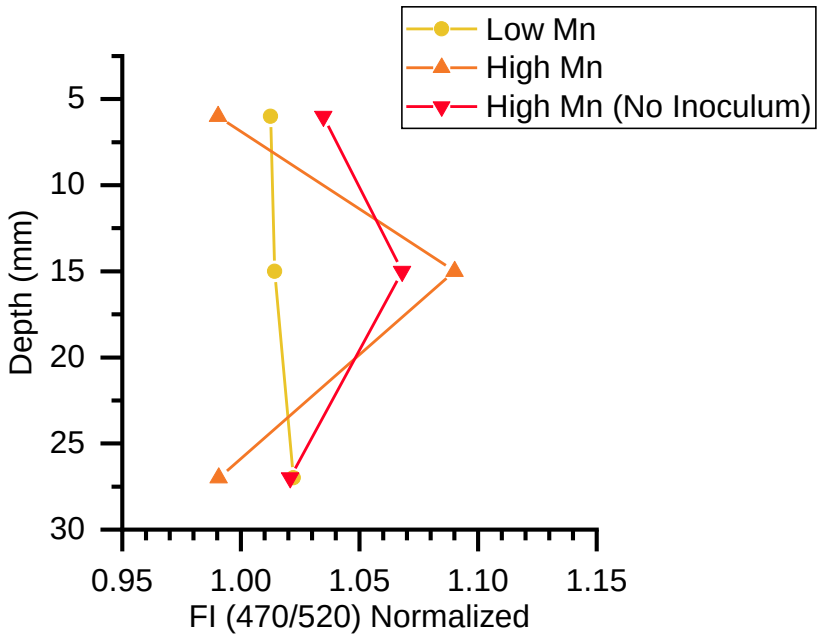

S.I. Figure 2. Fluorescence Index (FI) calculated between the ratio of emission at 470 nm and 520 nm normalized to the Control FI. Values are measured for the upper three sampling zone. A higher value indicates C attributed closer to microbial biomass.

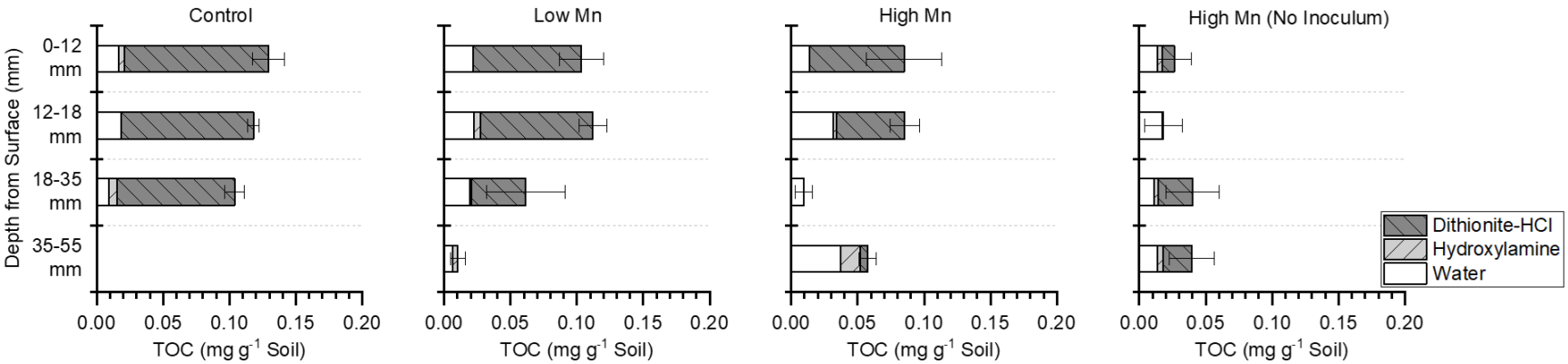

S.I. Figure 3. TOC analysis performed on a subsample of sequential extractions. Values are in mg C per gram soil extracted

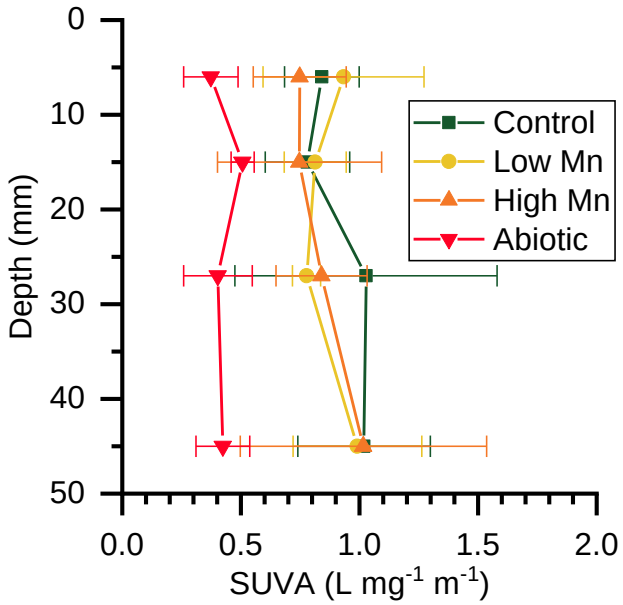

S.I. Figure 4. Change in aromaticity of OM within water extractions conducted using SUVA, calculated by normalizing UV_{254} by NPOC. A higher SUVA index is indicative of greater aromaticity in the sample. Here, there is great overlap in the SUVA index for all samples. The Abiotic treatment on average is characterized with a lower SUVA value, which would indicate it is less aromatic than the Mn treated reactors, contrary to our expectations.

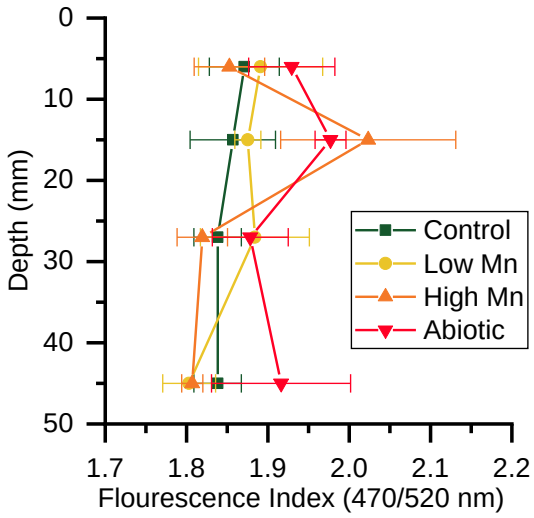

S.I. Figure 5. Change in predominant source of DOC determined using EEMs fluorescence index between 470 nm and 520 nm using an excitation of 370 nm. A higher ratio indicates the source of DOC to be attributed to microbial communities whereas a lower ratio has higher contribution from plant sources.

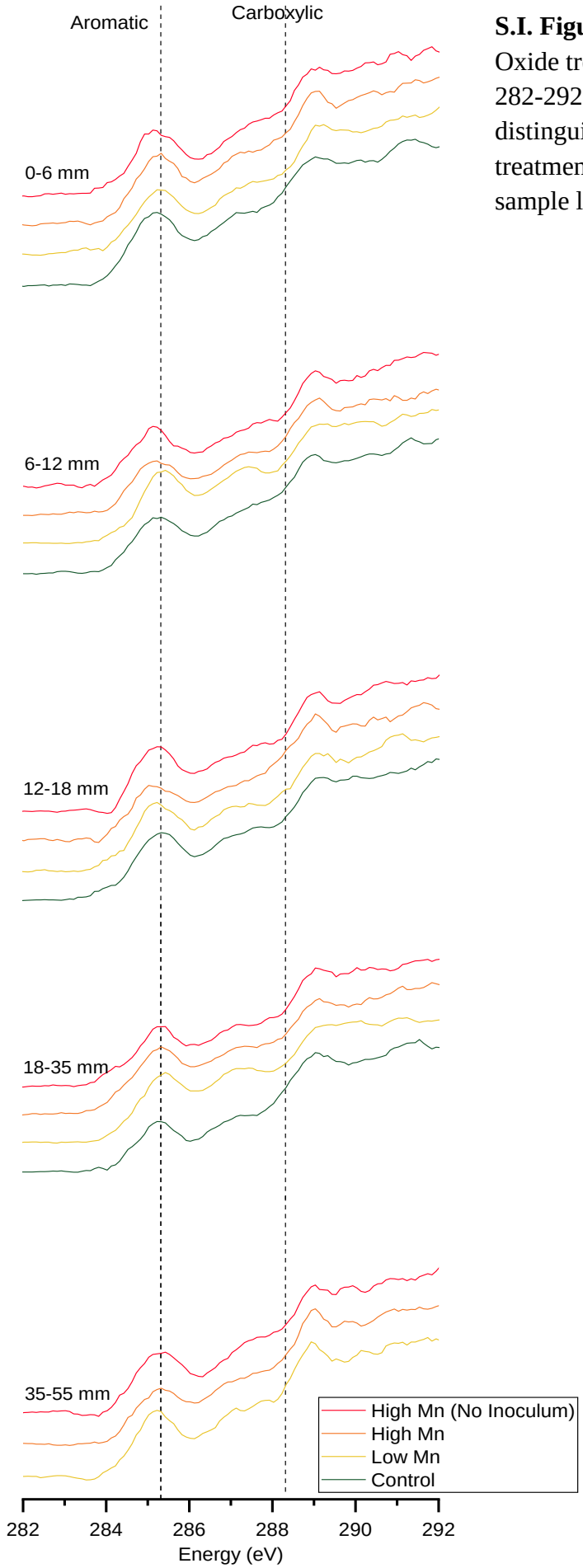

S.I. Figure 6 Stacked spectra for both the OAI and Mn Oxide treatment layer for all treatments, focused on the 282-292 eV region. Note that because we did not distinguish the 35-55 mm sampling zone for the Control treatment, there is no spectra relevant for that specific sample location.

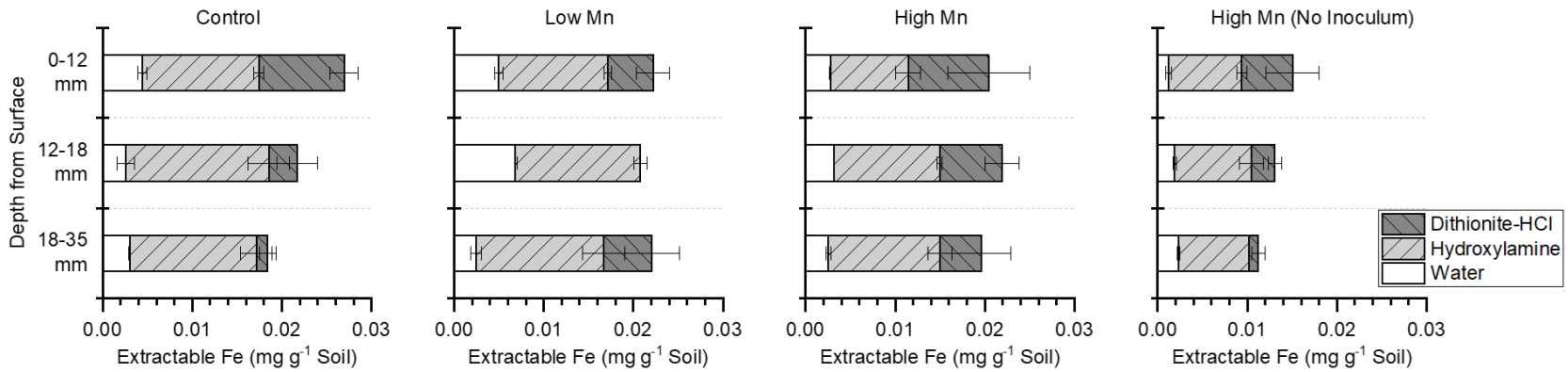

S.I. Figure 7 Sequential extraction results for Fe

SUPPLMENTARY FIGURES

Table S-1: Groundwater Concentrations Chemical constituents in artificial groundwater used during the reactor incubations, pH for the artificial groundwater solution was adjusted to 5.5 using NaOH and HS.

Compound	Concentration (mM)
KCl	4.155
$MgSO_4$	3.737
$CaSO_4 \cdot 2H_2O$	3.688
KH_2PO_4	0.0485
$NaHCO_3$	3.857
KNO_3	0.0732

Table S-2: C NEXAFS Fit Parameters

C Functional Group	eV
Quinonic	284.3
Aromatic	285.3
Phenolic	286.5
Aliphatic	287.5
Carboxylic	288.3
Alkylic	289
Carbonylic	290

Table S-3. Table of relative fit percentage for functional groups on C NEXAFS spectra along with Chi-squared goodness of fit:

Treatment	Sampling Zone (mm)	% Quinonic	% Aromatic	% Phenolic	% Aliphatic	% Carboxylic	% Alkylic	% Carbonylic	Chi-Squared
Control	0-6	3.5	22	10.5	17.7	7.9	30	8.4	0.78
	6-12	1.2	20.3	9.7	19	8.1	32.2	9.7	0.82
	12-18	2.3	21.7	10.8	19.1	4.3	31.1	10.8	0.58
	18-35	0	18.5	10.1	16.9	8	36.8	9.6	0.99
	35-55	-	-	-	-	-	-	-	-
Low Mn	0-6	2	21.5	9.3	20.5	2.9	33.8	10.1	0.71
	6-12	0.1	22.8	12	20.4	3.6	30.2	10.9	0.42
	12-18	2.4	23	11.6	18.7	4.7	30.9	8.8	1.39
	18-35	0.3	21.1	13.5	19.9	3.6	29.2	12.5	0.49
	35-55	0.2	21.2	9.3	19.1	6.7	34.5	9.1	1.39
High Mn	0-6	0.9	22.4	9.7	19.3	6.2	32.6	8.9	0.8
	6-12	2.1	20.1	9.4	18.8	5.7	33.8	10.2	1.21
	12-18	2.7	18.9	10.8	16.1	9.4	32.3	9.9	1.22
	18-35	3.3	21.4	12.6	18.4	5.5	29.8	9.1	0.59
	35-55	0	18.5	11.2	18.7	6.2	35.5	9.9	0.87
Abiotic	0-6	2.2	21.3	7.1	19.3	6.9	32	11.1	1.16
	6-12	3.7	22.1	8.2	19.3	3.9	34.2	8.6	1.73
	12-18	0	23.7	9.4	18.6	5.4	32.8	10.1	1.28
	18-35	2.4	19.2	11	17.7	5	32.8	11.8	0.75
	35-55	0	21.5	7.6	20.5	6.3	33.1	10.9	1.38

Table S-4. Statistical comparisons between individual extractions for corresponding sampling depths.

Water			
	0-12 mm	**12-18 mm**	**18-35 mm**
Comparison	**P-Value**	**P-Value**	**P-Value**
High v. Control	<0.01	0.02	0.85
High v. Low	0.79	0.38	0.97
High v. No Inoculum	<0.01	0.02	0.1
Low v. Control	<0.01	0.06	0.12
Low v. No Inoculum	<0.01	0.07	0.15
No Inoculum v. Control	0.99	0.99	0.99

Hydroxylamine			
	0-12 mm	**12-18 mm**	**18-35 mm**
Comparison	**P-Value**	**P-Value**	**P-Value**
High v. Control	<0.01	<0.01	0.15
High v. Low	0.65	0.18	0.7
High v. No Inoculum	0.02	<0.01	0.28
Low v. Control	0.02	0.02	0.42
Low v. No Inoculum	0.13	0.03	0.74
No Inoculum v. Control	0.6	0.95	0.9

Dithionite-HCl			
	0-12 mm	**12-18 mm**	**18-35 mm**
Comparison	**P-Value**	**P-Value**	**P-Value**
High v. Control	0.07	0.66	<0.01
High v. Low	0.3	0.87	0.98
High v. No Inoculum	0	0.99	1
Low v. Control	0.99	0.97	<0.01
Low v. No Inoculum	0.37	0.87	0.98
No Inoculum v. Control	0.09	0.66	<0.01

Table S-5. Statistical comparisons between modeled CO_2 data using an F-test for model fit

Single First Order Kinetic Model Comparison	
Comparison	**P-Value**
High v. Control	<0.01
High v. Low	<0.01
High v. No Inoculum	<0.01
Low v. Control	0.12
Low v. No Inoculum	<0.01
No Inoculum v. Control	<0.01

Table S-6. Comparisons between functional groups of the top 0-18mm (oxic and OAI). Total aromatic groups represent the sum of the relative abundance of quinonic, aromatic, and phenolic groups in C NEXAFS.

Treatment	Sampling Zone (mm)	Total Aromatic Groups (283.8 – 287 eV)	% Carboxylic	Carboxylic:Total Aromatic Groups
Control	0-18	33.9%	6.7%	0.20
Low Mn	0-18	34.9%	3.7%	0.11
High Mn	0-18	32.3%	7.1%	0.22
No Inoculum	0-18	32.6%	5.4%	0.17

BIBLIOGRAPHY

Aponte C, García L V., Marañón T (2012) Tree Species Effect on Litter Decomposition and Nutrient Release in Mediterranean Oak Forests Changes Over Time. Ecosystems 15:1204–1218. https://doi.org/10.1007/S10021-012-9577-4/FIGURES/5

Bengtson P, Bengtsson G (2007) Rapid turnover of DOC in temperate forests accounts for increased CO2 production at elevated temperatures. Ecol Lett 10:783–790. https://doi.org/10.1111/J.1461-0248.2007.01072.X

Berg B, Erhagen B, Johansson MB, et al (2015) Manganese in the litter fall-forest floor continuum of boreal and temperate pine and spruce forest ecosystems - A review. For. Ecol. Manage. 358:248–260

Berg B, Steffen KT, McClaugherty C (2007) Litter decomposition rate is dependent on litter Mn concentrations. Biogeochemistry. https://doi.org/10.1007/s10533-006-9050-6

Blume HP, Brümmer GW, Fleige H, et al (2015) Scheffer/schachtschabel soil science. Scheffer/Schachtschabel Soil Sci 1–618. https://doi.org/10.1007/978-3-642-30942-7/COVER

Bradford MA, Wieder WR, Bonan GB, et al (2016) Managing uncertainty in soil carbon feedbacks to climate change. Nat. Clim. Chang.

Burdige DJ, Dhakar SP, Nealson KH (2009) Effects of manganese oxide mineralogy on microbial and chemical manganese reduction. http://dx.doi.org.silk.library.umass.edu/101080/01490459209377902 10:27–48. https://doi.org/10.1080/01490459209377902

Chapnick SD, Moore WS, Nealson KH (1982) Microbially mediated manganese oxidation in a freshwater lake1. Limnol Oceanogr 27:1004–1014. https://doi.org/10.4319/LO.1982.27.6.1004

Davidson EA, Janssens IA (2006) Temperature sensitivity of soil carbon decomposition and feedbacks to climate change. https://doi.org/10.1038/nature04514

Dhandapani S, Evers S, Ritz K, Sjögersten S (2021) Nutrient and trace element concentrations influence greenhouse gas emissions from Malaysian tropical peatlands. Soil Use Manag 37:138–150. https://doi.org/10.1111/SUM.12669

Duckworth OW, Sposito G (2005) Siderophore-manganese (III) interactions. I. Air-oxidation of manganese(II) promoted by desferrioxamine B. Environ Sci Technol 39:6037–6044. https://doi.org/10.1021/es050275k

Froelich PN, Klinkhammer GP, Bender ML, et al (1979) Early oxidation of organic matter in pelagic sediments of the eastern equatorial Atlantic: suboxic diagenesis. Geochim Cosmochim Acta 43:1075–1090. https://doi.org/10.1016/0016-7037(79)90095-4

Gregory D, Carlson K (2003) Effect of soluble Mn concentration on oxidation kinetics. J Am Water Works Assoc 95:98–108. https://doi.org/10.1002/J.1551-8833.2003.TB10273.X

Hansel CM (2017) Manganese in Marine Microbiology. Adv Microb Physiol 70:37–83. https://doi.org/10.1016/BS.AMPBS.2017.01.005

Hättenschwiler S, Tiunov A V, Scheu S (2005) Biodiversity and Litter Decomposition in Terrestrial Ecosystems. Source Annu Rev Ecol Evol Syst 36:191–218. https://doi.org/10.1146/annurev.ecolsys.36.112904.151932

Heimann M, Reichstein M (2008) Terrestrial ecosystem carbon dynamics and climate feedbacks. Nature

Herndon EM, Jin L, Brantley SL (2011) Soils reveal widespread manganese enrichment from industrial inputs. Environ Sci Technol 45:241–247. https://doi.org/10.1021/ES102001W/SUPPL_FILE/ES102001W_SI_001.PDF

Hiroki M (2012) Effects of heavy metal contamination on soil microbial population. http://dx.doi.org/101080/00380768199210416961 38:141–147. https://doi.org/10.1080/00380768.1992.10416961

Hofrichter M (2002) Review: Lignin conversion by manganese peroxidase (MnP). Enzyme Microb. Technol.

Johnson JE, Savalia P, Davis R, et al (2016) Real-Time Manganese Phase Dynamics during Biological and Abiotic Manganese Oxide Reduction. Environ Sci Technol 50:4248–4258. https://doi.org/10.1021/ACS.EST.5B04834/ASSET/IMAGES/ES-2015-04834C_M003.GIF

Jones ME, Lacroix RE, Zeigler J, et al (2020) Enzymes, Manganese, or Iron? Drivers of Oxidative Organic Matter Decomposition in Soils. Environ Sci Technol 54:14114–14123. https://doi.org/10.1021/acs.est.0c04212

Jones ME, Nico PS, Ying S, et al (2018) Manganese-Driven Carbon Oxidation at Oxic-Anoxic Interfaces. Environ Sci Technol. https://doi.org/10.1021/acs.est.8b03791

Jones MR, Tebo BM (2021) Novel manganese cycling at very low ionic strengths in the Columbia River Estuary. Water Res 207:117801. https://doi.org/10.1016/J.WATRES.2021.117801

Keiluweit M, Nico P, Harmon ME, et al (2015) Long-term litter decomposition controlled by manganese redox cycling. Proc Natl Acad Sci U S A. https://doi.org/10.1073/pnas.1508945112

Keiluweit M, Wanzek T, Kleber M, et al (2017) Anaerobic microsites have an unaccounted role in soil carbon stabilization. Nat Commun 2017 81 8:1–10. https://doi.org/10.1038/s41467-017-01406-6

Kim B, Lingappa UF, Magyar J, et al (2022) Challenges of Measuring Soluble Mn(III) Species in Natural Samples. Molecules 27:. https://doi.org/10.3390/MOLECULES27051661

Kirker G, Zelinka S, Gleber SC, et al (2017) Synchrotron-based X-ray fluorescence microscopy enables multiscale spatial visualization of ions involved in fungal lignocellulose deconstruction. Sci Rep. https://doi.org/10.1038/srep41798

Kranabetter JM (2019) Increasing soil carbon content with declining soil manganese in temperate rainforests: is there a link to fungal Mn? Soil Biol Biochem 128:179–181. https://doi.org/10.1016/J.SOILBIO.2018.11.001

LaRowe DE, Carlson HK, Amend JP (2021) The Energetic Potential for Undiscovered Manganese Metabolisms in Nature. Front Microbiol 12:1347. https://doi.org/10.3389/FMICB.2021.636145/BIBTEX

Li H, Santos F, Butler K, Herndon E (2021a) A Critical Review on the Multiple Roles of Manganese in Stabilizing and Destabilizing Soil Organic Matter. Environ Sci Technol 55:12136–12152. https://doi.org/10.1021/acs.est.1c00299

Li H, Santos F, Butler K, Herndon E (2021b) A Critical Review on the Multiple Roles of Manganese in Stabilizing and Destabilizing Soil Organic Matter. Cite This Environ Sci Technol 55:12136–12152. https://doi.org/10.1021/acs.est.1c00299

Luther GW, Popp JI (2002) Kinetics of the Abiotic Reduction of Polymeric Manganese Dioxide by Nitrite: An Anaerobic Nitrification Reaction. Aquat Geochemistry 2002 81 8:15–36. https://doi.org/10.1023/A:1020325604920

Ma D, Wu J, Yang P, Zhu M (2020) Coupled Manganese Redox Cycling and Organic Carbon Degradation on Mineral Surfaces. Environ Sci Technol 54:8801–8810. https://doi.org/10.1021/ACS.EST.0C02065/SUPPL_FILE/ES0C02065_SI_001.PDF

Ma D, Wu J, Yang P, Zhu M (2022) Coupled Manganese Redox Cycling and Organic Carbon Degradation on Mineral Surfaces. Environ Sci Technol 54:16. https://doi.org/10.1021/acs.est.0c02065

Madison AS, Tebo BM, Mucci A, et al (2013) Abundant porewater Mn(III) is a major component of the sedimentary redox system. Science (80-). https://doi.org/10.1126/science.1241396

Manceau A, Marcus MA, Grangeon S (2012) Determination of Mn valence states in mixed-valent manganates by XANES spectroscopy. Am Mineral 97:816–827. https://doi.org/10.2138/AM.2012.3903/MACHINEREADABLECITATION/RIS

Meentemeyer V (1978) Macroclimate and Lignin Control of Litter Decomposition Rates. Ecology 59:465–472. https://doi.org/10.2307/1936576

Morgan JJ, Schlautman MA, Bilinski H (2021) Rates of Abiotic MnIIOxidation by O2: Influence of Various Multidentate Ligands at High pH. Environ Sci Technol 55:14426–14435. https://doi.org/10.1021/ACS.EST.1C01795/ASSET/IMAGES/LARGE/ES1C01795_0003.JPEG

Nealson KH, Myers CR (1992) Microbial reduction of manganese and iron: New approaches to carbon cycling. Appl. Environ. Microbiol.

Oldham VE, Jones MR, Tebo BM, Luther GW (2017a) Oxidative and reductive processes contributing to manganese cycling at oxic-anoxic interfaces. Mar Chem. https://doi.org/10.1016/j.marchem.2017.06.002

Oldham VE, Jones MR, Tebo BM, Luther GW (2017b) Oxidative and reductive processes contributing to manganese cycling at oxic-anoxic interfaces. Mar Chem 195:122–128. https://doi.org/10.1016/J.MARCHEM.2017.06.002

Perez J, Jeffries TW (1992) Roles of manganese and organic acid chelators in regulating lignin degradation and biosynthesis of peroxidases by Phanerochaete chrysosporium. Appl Environ Microbiol. https://doi.org/10.1128/aem.58.8.2402-2409.1992

Pinzari F, Cuadros J, Migliore M, et al (2018) Manganese translocation and concentration on Quercus cerris decomposing leaf and wood litter by an ascomycetous fungus: an active process with ecosystem consequences? FEMS Microbiol Ecol 94:. https://doi.org/10.1093/femsec/fiy111

Rajapaksha RMCP, Tobor-Kapłon MA, Bååth E (2004) Metal toxicity affects fungal and bacterial activities in soil differently. Appl Environ Microbiol 70:2966–2973. https://doi.org/10.1128/AEM.70.5.2966-2973.2004/ASSET/5F99ADA9-1D33-44E7-AF94-ECB469C8A44C/ASSETS/GRAPHIC/ZAM0050444210007.JPEG

Ravel B, Newville M (2005) ATHENA, ARTEMIS, HEPHAESTUS: Data analysis for X-ray absorption spectroscopy using IFEFFIT. J Synchrotron Radiat 12:537–541. https://doi.org/10.1107/S0909049505012719

Reith F, Drake HL, KÃ¼sel K (2002) Anaerobic activities of bacteria and fungi in moderately acidic conifer and deciduous leaf litter. FEMS Microbiol Ecol 41:27–35. https://doi.org/10.1111/J.1574-6941.2002.TB00963.X

Rennert T, Händel M, Höschen C, et al (2014) A NanoSIMS study on the distribution of soil organic matter, iron and manganese in a nodule from a Stagnosol. Eur J Soil Sci 65:684–692. https://doi.org/10.1111/EJSS.12157

Sanchez M, Benjamin J, Turner L Abiotic contribution to phenol oxidase activity across a manganese gradient in tropical forest soils. https://doi.org/10.1007/s10533-021-00764-0

Scharlemann JPW, Tanner EVJ, Hiederer R, Kapos V (2014) Global soil carbon: Understanding and managing the largest terrestrial carbon pool. Carbon Manag.

Sleutel S, De Neve S, Prat Roibás MR, Hofman G (2005) The influence of model type and incubation time on the estimation of stable organic carbon in organic materials. Eur J Soil Sci 56:505–514. https://doi.org/10.1111/J.1365-2389.2004.00685.X

Stendahl J, Berg B, Lindahl BD (2017) Manganese availability is negatively associated with carbon storage in northern coniferous forest humus layers. Sci Rep. https://doi.org/10.1038/s41598-017-15801-y

Stone AT (1987) Microbial metabolites and the reductive dissolution of manganese oxides: Oxalate and pyruvate. Geochim Cosmochim Acta 51:919–925. https://doi.org/10.1016/0016-7037(87)90105-0

Sun T, Cui Y, Berg B, et al (2019) A test of manganese effects on decomposition in forest and cropland sites. Soil Biol Biochem. https://doi.org/10.1016/j.soilbio.2018.11.018

Tebo BM (1991) Manganese(II) oxidation in the suboxic zone of the Black Sea. Deep Sea Res Part A Oceanogr Res Pap 38:S883–S905. https://doi.org/10.1016/S0198-0149(10)80015-9

Thompson IA, Huber DM, Guest CA, Schulze DG (2005) Fungal manganese oxidation in a reduced soil. Environ Microbiol. https://doi.org/10.1111/j.1462-2920.2005.00842.x

Tian G, Kang BT, Brussaard L (1992) Biological effects of plant residues with contrasting chemical compositions under humid tropical conditions—Decomposition and nutrient release. Soil Biol Biochem 24:1051–1060. https://doi.org/10.1016/0038-0717(92)90035-V

Trouwborst RE, Clement BG, Tebo BM, et al (2006) Soluble Mn(III) in suboxic zones. Science (80-). https://doi.org/10.1126/science.1132876

Trum F, Titeux H, Ponette Q, Berg B (2015) Influence of manganese on decomposition of common beech (Fagus sylvatica L.) leaf litter during field incubation. Biogeochemistry. https://doi.org/10.1007/s10533-015-0129-9

Van Der Lee GEM, De Winder B, Bouten W, Tietema A (1999) Anoxic microsites in Douglas fir litter. Soil Biol Biochem 31:1295–1301. https://doi.org/10.1016/S0038-0717(99)00048-6

Villalobos M, Toner B, Bargar J, Sposito G (2003) Characterization of the manganese oxide produced by Pseudomonas putida strain MnB1. Geochim Cosmochim Acta 67:2649–2662. https://doi.org/10.1016/S0016-7037(03)00217-5

Warrinnier R, Bossuyt S, Resseguier C, et al (2020) Anaerobic Respiration in the Unsaturated Zone of Agricultural Soil Mobilizes Phosphorus and Manganese. Cite This Environ Sci Technol 54:4931. https://doi.org/10.1021/acs.est.9b06978

Whalen ED, Smith RG, Grandy AS, Frey SD (2018) Manganese limitation as a mechanism for reduced decomposition in soils under atmospheric nitrogen deposition. https://doi.org/10.1016/j.soilbio.2018.09.025

Yue K, Ni X, Fornara DA, et al (2021) Dynamics of Calcium, Magnesium, and Manganese During Litter Decomposition in Alpine Forest Aquatic and Terrestrial Ecosystems. Ecosystems 24:516–529. https://doi.org/10.1007/S10021-020-00532-5

Zeiner CA, Purvine SO, Zink EM, et al (2016) Comparative analysis of secretome profiles of manganese(II)-oxidizing Ascomycete fungi. PLoS One. https://doi.org/10.1371/journal.pone.0157844

Zelinka SL, Jakes JE, Kirker GT, et al (2021) Oxidation states of iron and manganese in lignocellulose altered by the brown rot fungus Gloeophyllum trabeum measured in-situ using X-ray absorption near edge spectroscopy (XANES). Int Biodeterior Biodegrad. https://doi.org/10.1016/j.ibiod.2020.105162